

# Non-planar elasticae as optimal curves for the magnetic axis of stellarators

D. Pfefferlé,<sup>1</sup> L. Gunderson,<sup>2</sup> S.R. Hudson,<sup>2</sup> and L. Noakes<sup>1</sup>

<sup>1</sup>*The University of Western Australia, 35 Stirling Highway, Crawley WA 6009, Australia*

<sup>2</sup>*Princeton Plasma Physics Laboratory, Princeton, New Jersey 08543, USA*

(Dated: March 15, 2022)

The problem of finding an optimal curve for the target magnetic axis of a stellarator is addressed. Euler-Lagrange equations are derived for finite length three-dimensional curves that extremise their bending energy while yielding fixed integrated torsion. The obvious translational and rotational symmetry is exploited to express solutions in a preferred cylindrical coordinate system in terms of elliptic Jacobi functions. These solution curves, which, up to similarity transformations, depend on three dimensionless parameters, do not necessarily close. Two closure conditions are obtained for the vertical and toroidal displacement (the radial coordinate being trivially periodic) to yield a countably infinite set of one-parameter families of closed non-planar curves. The behaviour of the integrated torsion (Twist of the Frenet frame), the Linking of the Frenet frame and the Writhe of the solution curves is studied in light of the Călugăreanu theorem. A refreshed interpretation of Mercier's formula for the on-axis rotational transform of stellarator magnetic field-lines is proposed.

Keywords: stellarator design, variational principle, non-planar curves, elastica, linking, writhing, twisting

## I. INTRODUCTION

In toroidal fusion devices such as the tokamak and the stellarator, high rotational transform - the average linking of neighbouring field-lines per revolution around the axis - is essential for plasma confinement [1]. In tokamaks, which are axisymmetric devices, the winding of the magnetic field is obtained by varying the poloidal flux in time, thereby inducing strong toroidal (parallel) currents (or curl of the inner magnetic field). The duration of a tokamak discharge is thus limited to the duration of the ramp-up and ramp-down of the central solenoid stack, although there are ways to sustain current through radio waves (cyclotron resonance) [2] or by exploiting kinetic effects (bootstrap) [3]. In stellarators, the confining field is static and net toroidal currents are avoided. The external current-carrying coils are arranged in such a way that the vacuum magnetic field produced wraps tightly around the plasma, thereby linking the magnetic axis by the helical trajectory of its field-lines. The main reason the production cost of a stellarator is so high is because the shape of its coils can be extremely complex. Optimising the coil geometry is an important component of stellarator design [4] and a prerequisite for the economic viability of the stellarator concept.

The stellarator optimisation problem is extremely difficult in that the number of degrees of freedom is far too large to be explored empirically; design points must be chosen through well-organised computations [5]. A potential caveat is that the choice of coordinates and magnetic field representation will favour certain classes of solutions. For example, a Fourier expansion in terms of the toroidal angle will not allow for plasma shapes with vertical or radial portions, although it is entirely possible that such configurations can result in simpler coils and better confinement performances. In this sense, numerical computations must be guided by the theoretical understanding of simple models, that can serve as reliable

benchmark cases for code verification and validation.

It is common knowledge that high rotational transform at the magnetic axis of stellarators can be achieved without inducing current by means of two independent effects [6, 7]: i) rotating an elliptic plasma boundary along a circular (planar) axis, as for example in the Large Helical Device (LHD) in Toki, Japan [8], ii) harnessing finite integrated torsion from a non-planar magnetic axis, as for example in the Wendelstein 7-X in Greifswald, Germany [9]. In the first case, penetration of the helical component is expected to decay as  $r^{m-1}$ , where  $r$  is the minor radius of the torus and  $m$  is the poloidal mode number of the applied boundary rotation (for an elliptic boundary  $m = 2$ ). The plasma edge thus receives more shear than the axis. In the second case, the rotational transform at the magnetic axis arises purely from its geometry. It can be imposed, up to a certain extent, almost independently from the rotation of the boundary. A recent coil design exercise using the FOCUS code [10] has shown that increasing ellipticity of the boundary tends to increase the coil complexity more so than increasing the integrated torsion [11].

It is thus legitimate to ask what smooth curve provides maximum integrated torsion without being too “complex”. More precisely: What are the closed curves of fixed length and given integrated torsion that minimise bending energy? This particular question is addressed in a series of mathematical papers [12–14]. The analysis therein is repeated and extended with a focus on being able to control the integrated torsion of the magnetic axis and produce a maximum amount of rotational transform. The representation of solution curves is exploited to categorise families of ideal target magnetic axes and starting points for efficient stellarator designs. Our derivation deviates from [14] in the fact that the length of the curve is held fixed and the maximum curvature becomes a dependent variable, whereas the opposite assumption is made in their work.

The strategy is to first obtain the solution to the variational problem of minimising the total squared curvature of a curve with fixed length and prescribed integrated torsion. The solution curves do not necessarily close on themselves, therefore additional conditions are derived to constrain the set of free parameters. The result is a countably infinite set of one-parameter families of closed curves isotopic to torus knots (including the unknot). It is then highlighted that smooth deformations of the solution curves near states of inflexion give rise to severe discontinuities in the integrated torsion, which on physical grounds cannot affect the on-axis rotational transform. This inconsistency is resolved by applying the Călugăreanu theorem to the linking of magnetic field-lines separately to the linking of the Frenet frame on the magnetic axis. In fact, it is shown that the relevant quantity for the on-axis rotational transform due to non-planar geometry is the so-called *Writhe* of the supporting curve. A quantitative estimate of the Writhe (and consequently the on-axis rotational transform) is derived for our closed energy-minimising (elastic) curves. The well-known formula by Mercier [6] is revisited to provide a clear interpretation of its mysterious integer of topological origin.

After some definitions, section II recalls the properties of the Frenet frame for three-dimensional curves. Section III formulates the variational problem of minimising bending energy subject to constraints on length and integrated torsion, and derives the associated Euler-Lagrange equations. Section IV exploits the symmetries of the Lagrangian in order to yield two Noether fields. Section V derives analytic solutions to the Euler-Lagrange equations in a special cylindrical coordinate system. Section VI lists a series of conditions for the solution curves to be periodic and closed. Section VII assesses the integrated torsion and expresses the linking of the Frenet frame as well as the Writhe of closed solution curves based on the Călugăreanu theorem. The effect of non-planar geometry on the on-axis rotational transform is quantified for  $n$ -periodic unknotted closed solution curves and the conjugate  $(n-1, n)$ -torus knots. Section VIII concludes the work.

## II. DEFINITIONS

The target magnetic axis of a stellarator is represented by a smooth curve  $\mathbf{x}(s)$  (of class  $C^\infty$ ), parametrised by its arc-length  $s \in [0, L]$ , where  $L$  is its total length. This representation is such that the velocity vector has unit length,

$$\mathbf{x}' \cdot \mathbf{x}' = 1, \quad (1)$$

where  $\mathbf{x}' = d\mathbf{x}/ds$ . One can verify that there is no loss of generality in choosing the arc-length parametrisation, only for an explicit constraint (Lagrange multiplier function) appearing in the variational formulation; the same Euler-Lagrange equations are obtained starting with an

arbitrary parametrisation where only the length of the curve is constrained [13]. The arc-length parametrisation significantly reduces the algebra.

The fundamental theorem of curves states that every regular curve in  $\mathbb{R}^3$  with non-zero curvature is completely determined up to isometries by its curvature and torsion functions, respectively  $\kappa$  and  $\tau$ , via the Frenet-Serret formulae,

$$\begin{pmatrix} \mathbf{x} \\ \mathbf{t} \\ \mathbf{n} \\ \mathbf{b} \end{pmatrix}' = \begin{pmatrix} 0 & 1 & 0 & 0 \\ 0 & 0 & \kappa & 0 \\ 0 & -\kappa & 0 & \tau \\ 0 & 0 & -\tau & 0 \end{pmatrix} \begin{pmatrix} \mathbf{x} \\ \mathbf{t} \\ \mathbf{n} \\ \mathbf{b} \end{pmatrix}, \quad (2)$$

where  $\{\mathbf{t}, \mathbf{n}, \mathbf{b}\}$  - the tangent, normal, and bi-normal vector triad - forms the orthonormal Frenet frame,

$$\begin{aligned} \mathbf{x}' &\stackrel{(1)}{=} \mathbf{t} \\ \mathbf{x}'' &= \mathbf{t}' = \kappa \mathbf{n} \\ \mathbf{x}''' &= -\kappa^2 \mathbf{t} + \kappa' \mathbf{n} + \kappa \tau \mathbf{b} \\ \mathbf{x}'''' &= -3\kappa' \kappa \mathbf{t} + (\kappa'' - \kappa^3 - \kappa \tau^2) \mathbf{n} + (2\kappa' \tau + \kappa \tau') \mathbf{b} \end{aligned} \quad (3)$$

where  $\mathbf{b} = \mathbf{t} \times \mathbf{n}$ .

The curvature and torsion of the curve correspond to

$$\kappa^2(\mathbf{x}'') = \mathbf{x}'' \cdot \mathbf{x}'' \stackrel{(1)}{=} -\mathbf{x}' \cdot \mathbf{x}''', \quad (4)$$

$$\tau(\mathbf{x}', \mathbf{x}'', \mathbf{x}''') = \frac{(\mathbf{x}' \times \mathbf{x}'') \cdot \mathbf{x}'''}{\kappa^2}. \quad (5)$$

These functions are noted to scale with the inverse of the curve's length, i.e.  $\kappa \propto \tau \propto L^{-1}$ . This fact is used later to adimensionalise the parameter space of the solution curves. The following identities are also listed for later use:

$$\frac{\partial \tau}{\partial \mathbf{x}'} = \tau \mathbf{t} + \kappa \mathbf{b}, \quad \left( \frac{\partial \tau}{\partial \mathbf{x}'} \right)' = \tau' \mathbf{t} + \kappa' \mathbf{b}, \quad (6)$$

$$\frac{\partial \tau}{\partial \mathbf{x}''} = -\frac{\tau}{\kappa} \mathbf{n} - \frac{\kappa'}{\kappa^2} \mathbf{b}, \quad \frac{\partial \tau}{\partial \mathbf{x}'''} = \frac{1}{\kappa} \mathbf{b}, \quad (7)$$

$$\frac{\partial \tau}{\partial \mathbf{x}''} = \left( \frac{\partial \tau}{\partial \mathbf{x}'''} \right)'. \quad (8)$$

Owing to the classical Euler-Bernoulli model of thin elastic rods, we consider the *bending energy* of a curve to be proportional to the total squared curvature,

$$\mathcal{E} := \int_0^L \frac{1}{2} \kappa^2 ds = \int_0^L \frac{1}{2} \mathbf{x}'' \cdot \mathbf{x}'' ds, \quad (9)$$

as a measure of the complexity of the magnetic field and therefore a component of the total cost of the coil design.

Critical points of the bending energy functional for given boundary conditions are well-known curves called *elasticae* and have been extensively studied in the context of beam deflection. Among all closed curves, Fenchel's theorem [15] states that  $\mathcal{E} \geq 4\pi^2/L$ , where the lower bound is achieved by the planar circle - the most trivial closed elastica with constant curvature and zero torsion.

Interestingly, there is a countably infinite set of closed non-circular elasticae [12], which however correspond to "saddle points" of the bending energy functional [16]. A constraint on the non-planarity thus needs to be added to the variational problem in order to yield stable non-planar optimal stellarator axes. A convenient choice is to control the *average torsion*, referred hereafter by the following dimensional quantity

$$\langle \tau \rangle := \frac{1}{L} \int_0^L \tau ds. \quad (10)$$

We will refer to the *integrated torsion* - or the *Twist of the Frenet frame* - by the adimensional quantity

$$\mathcal{T}_{w,\text{Frenet}} := \frac{1}{2\pi} \int_0^L \tau ds = \frac{L}{2\pi} \langle \tau \rangle. \quad (11)$$

### III. EULER-LAGRANGE EQUATIONS

The curve of minimal bending energy and prescribed integrated torsion is the extremal curve of the objective functional

$$S[\mathbf{x}] = \int_0^L ds \left[ \frac{1}{2} \kappa^2 + \frac{1}{2} \Lambda(\mathbf{x}' \cdot \mathbf{x}' - 1) + \lambda_2(\tau - \tau_0) \right], \quad (12)$$

which consists of three terms: i) the bending energy, ii) a term enforcing the arc-length parametrisation of equation (1) via the Lagrange multiplier function  $\Lambda(s)$  and iii) a term to control the integrated torsion via the scalar Lagrange multiplier  $\lambda_2$ , so that  $\langle \tau \rangle = \tau_0$ . The relative sign between the terms is absorbed in the Lagrange multipliers. The whole integrand is commonly referred to as the *Lagrangian*.

Variation of the functional  $S$  with respect to  $\mathbf{x}$  yields

$$\delta S = \int_0^L ds \left\{ \mathbf{E} \cdot \delta \mathbf{x} + \frac{d}{ds} \left[ \lambda_2 \frac{\partial \tau}{\partial \mathbf{x}'''} \cdot \delta \mathbf{x}'' + \mathbf{x}'' \cdot \delta \mathbf{x}' + \left( -\mathbf{x}''' + \Lambda \mathbf{x}' + \lambda_2 \frac{\partial \tau}{\partial \mathbf{x}'} \right) \cdot \delta \mathbf{x} \right] \right\}, \quad (13)$$

where the Euler-Lagrange equations are identified as

$$\mathbf{E}(\mathbf{x}', \mathbf{x}'', \mathbf{x}''', \mathbf{x}'''' ) = \mathbf{x}'''' - (\Lambda \mathbf{x}')' - \lambda_2 \left( \frac{\partial \tau}{\partial \mathbf{x}'} \right)' = 0. \quad (14)$$

A simplification occurred thanks to (8). The differential vector equation (14) can be written in terms of the curvature and torsion functions in the Frenet frame, as

$$-(\Lambda' + 3\kappa'\kappa + \lambda_2\tau')\mathbf{t} + (\kappa'' - \kappa^3 - \kappa\tau^2 - \Lambda\kappa)\mathbf{n} + [\kappa'(2\tau - \lambda_2) + \kappa\tau']\mathbf{b} = 0. \quad (15)$$

After integrating once, this leads to the following relations:

$$\Lambda(s) = \lambda_1 - \frac{3}{2}\kappa^2 - \lambda_2\tau, \quad (16)$$

$$\kappa^2(2\tau - \lambda_2) = c, \quad (17)$$

$$(\kappa')^2 + \frac{1}{4}(\kappa^2 - 2\lambda_1)^2 + \kappa^2(\tau - \lambda_2)^2 = J^2, \quad (18)$$

where  $\lambda_1$  is a scalar Lagrange multiplier related to the constraint on total length, and  $c$  and  $J^2$  are integration constants. The four parameters,  $\lambda_1$ ,  $\lambda_2$ ,  $c$  and  $J^2$ , completely determine the size and shape of the solution to the Euler-Lagrange equations (up to isometries) [14].

### IV. SYMMETRIES AND NOETHER CHARGES

The Euler-Lagrange equation (14) can be immediately integrated to yield  $\mathbf{x}''' - \Lambda \mathbf{x}' - \lambda_2 \left( \frac{\partial \tau}{\partial \mathbf{x}'} \right) = \mathbf{J}$ , where  $\mathbf{J}$  is the constant force from the end points propagating along the curve. Translations and rotations constitute isometries in  $\mathbb{R}^3$  and are obvious symmetries of the Lagrangian. From Noether's theorem, one learns that  $\mathbf{J}$  represents the conserved quantity related to the invariance of the Lagrangian under translations,  $\delta \mathbf{x} = \mathbf{\Delta}$ ,  $\delta \mathbf{x}' = \delta \mathbf{x}'' = 0$  where  $\mathbf{\Delta}$  is an arbitrary constant vector. Thus, the curve is such that the following vector field is constant:

$$\mathbf{J} = \frac{1}{2}(\kappa^2 - 2\lambda_1)\mathbf{t} + \kappa'\mathbf{n} + \kappa(\tau - \lambda_2)\mathbf{b}. \quad (19)$$

Thanks to the invariance of the Lagrangian under rotation,  $\delta \mathbf{x} = \mathbf{\Omega} \times \mathbf{x}$ ,  $\delta \mathbf{x}' = \mathbf{\Omega} \times \mathbf{x}'$  and  $\delta \mathbf{x}'' = \mathbf{\Omega} \times \mathbf{x}''$  where  $\mathbf{\Omega}$  is an arbitrary constant vector, we obtain another Noether charge  $\mathbf{A}$ , related to the torque from the end points. Therefore, the curve is such that the following vector field,

$$\mathbf{I}(s) = \lambda_2 \mathbf{t} + \kappa \mathbf{b} = \mathbf{A} + \mathbf{x} \times \mathbf{J} \quad (20)$$

generates an isometry (translation along  $\mathbf{A}$  and rotation around  $\mathbf{J}$ ). We see from (20) that, under translation  $\mathbf{x} \mapsto \mathbf{x} + \mathbf{\Delta}$ ,  $\mathbf{A} \mapsto \mathbf{A} - \mathbf{\Delta} \times \mathbf{J}$ . By choosing  $\mathbf{\Delta} = \mathbf{J} \times \mathbf{A} / J^2$ , the charge  $\mathbf{A} \mapsto \mathbf{J}(\mathbf{A} \cdot \mathbf{J}) / J^2$  can be aligned with  $\mathbf{J}$ , such that only the only relevant component is

$$\mathbf{A} \cdot \mathbf{J} = \mathbf{I} \cdot \mathbf{J} = \frac{1}{2}c - \lambda_1\lambda_2 := aJ^2. \quad (21)$$

By virtue of rotational invariance, we mention that the solution curves respect *stellarator symmetry* [17], which is equivalent to a 180-degree rotation about a characteristic axis in the  $xy$  plane.

Reparametrisation of the curve does not affect its properties. In particular, the reversal of the arc-length  $s \mapsto -s$  together with  $\mathbf{J} \mapsto -\mathbf{J}$ ,  $\mathbf{A} \mapsto -\mathbf{A}$  and  $\tau_0 \mapsto -\tau_0$  represent the same solution. Furthermore, the Lagrangian is invariant under a parity transformation  $\mathbf{x} \mapsto -\mathbf{x}$  together with  $\tau_0 \mapsto -\tau_0$ ,  $\lambda_2 \mapsto -\lambda_2$ ,  $c \mapsto -c$  and  $\mathbf{J} \mapsto -\mathbf{J}$ . Solution curves with negative integrated torsion can be related to the ones with positive via orthogonal (rotation and parity) and arc-length-reversal transformations.

## V. ANALYTIC SOLUTION

### A. Curvature function

Equations (17-18) admit the following solution [14],

$$\kappa^2(s) = \kappa_0^2 \left[ 1 - \frac{p^2}{w^2} \text{sn}^2(t, p) \right], \quad t = \frac{\kappa_0}{2w}(s - s_0), \quad (22)$$

where  $\text{sn}(t, p)$  is the Jacobi Elliptic sine function satisfying  $(d\text{sn}/dt)^2 = (1 - \text{sn}^2)(1 - p^2 \text{sn}^2)$ . The maximum curvature  $\kappa_0 > 0$  and parameters  $0 \leq p \leq w \leq 1$  are (non-linearly) related to the original set through

$$4\lambda_1 - \lambda_2^2 = \frac{\kappa_0^2}{w^2}(3w^2 - p^2 - 1), \quad (23)$$

$$c^2 = \frac{\kappa_0^6}{w^4}(w^2 - p^2)(1 - w^2), \quad (24)$$

$$4J^2 = (\kappa_0^2 - 2\lambda_1)^2 + \kappa_0^2 \left( \frac{c}{\kappa_0^2} - \lambda_2 \right)^2. \quad (25)$$

Since  $\kappa_0 \propto L^{-1}$ , the following adimensional parameters are used to factor out the uniform scaling of solutions:

$$\bar{c} = c/\kappa_0^3, \quad \bar{J} = J/\kappa_0^2, \quad \bar{a} = a\kappa_0, \quad (26)$$

$$\bar{\lambda}_1 = \lambda_1/\kappa_0^2, \quad \bar{\lambda}_2 = \lambda_2/\kappa_0. \quad (27)$$

Then, only three (adimensional) parameters are required to specify the solution curves up to similarity transformations.

In anticipation of later results, we define

$$X = \bar{\lambda}_2 w, \quad Y = \frac{\bar{c} w^2}{\sqrt{1 - w^2}}, \quad (28)$$

and consider  $(X, Y, p^2)$  as our independent (dimensionless) parameters. For convenience, we also define the radius  $R$  in  $(X, Y)$ -space,

$$R^2 = X^2 + Y^2. \quad (29)$$

Curves with  $X = 0$  correspond to classical elasticae, where the Lagrange multiplier on torsion vanishes,  $\lambda_2 = 0$ . Those solutions are discussed in detail in [12]. Curves with  $Y = 0$  have constant torsion ( $c = 0$ ) and are called elastic rods.

A parity transformation in real space corresponds to a point reflection of coordinates  $(X, Y) \mapsto (-X, -Y)$ . Parity invariance implies symmetry (or anti-symmetry) of all features in the  $(X, Y)$  plane under a 180-degree rotation, as illustrated in the figures below.

Based on the set of parameters  $(X, Y, p^2)$ , equation (24) becomes an equation for  $w^2$ ,

$$w^2 = Y^2 + p^2, \quad (30)$$

showing that the parameter  $Y \in [-p', p']$  is bounded, where  $p' = \sqrt{1 - p^2}$ . Equation (23) becomes an equation for  $\bar{\lambda}_1$ ,

$$\bar{\lambda}_1 = \frac{1}{2} - \frac{1 - R^2}{4w^2} \quad \text{or} \quad 1 - 2\bar{\lambda}_1 = \frac{1 - R^2}{2w^2}. \quad (31)$$

Equation (25) becomes an equation for  $\bar{J}$ ,

$$\bar{J} = \pm \frac{\sqrt{(1 - R^2)^2 + 4(Yw' - Xw)^2}}{4w^2}, \quad (32)$$

where  $w' = \sqrt{1 - w^2}$ . Equation (21) becomes an equation for  $\bar{a}$ , which we express as

$$U = w\bar{a}\bar{J} = \frac{X(1 - R^2) + 2(Yw' - Xw)w}{4\bar{J}w^2}. \quad (33)$$

It is convenient to define the conjugate of  $U$ ,

$$V = \frac{Y(1 - R^2) - 2(Yw' - Xw)w'}{4\bar{J}w^2}, \quad (34)$$

such that  $U^2 + V^2 = X^2 + Y^2 = R^2$ .

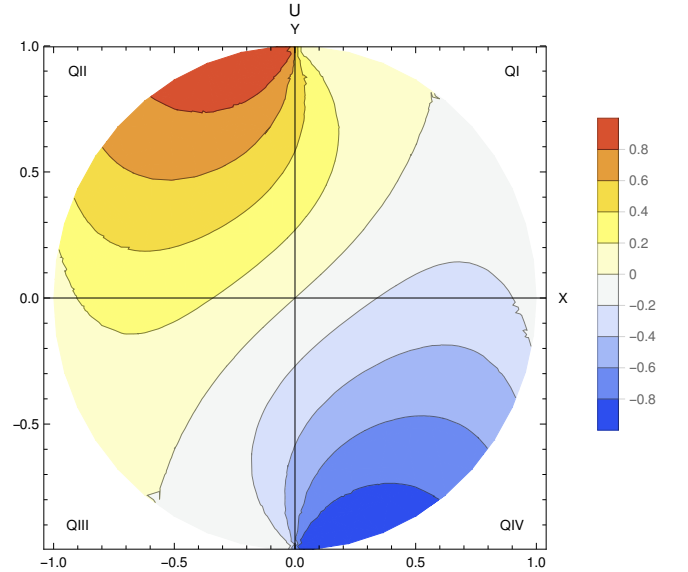


FIG. 1. Contours of constant  $U$  under the closure condition  $\Delta z = 0$ .

### B. Cylindrical coordinates

Exploiting the freedom of choosing the origin and orientation of the coordinate system (translational and rotational symmetry), we may align both constants of motion,  $\mathbf{J} = J\hat{z}$  and  $\mathbf{A} = a\mathbf{J} = aJ\hat{z}$  along the vertical axis. We will assume that  $J > 0$  defines the vertical direction whereas  $a$  can be positive or negative (the other branch of solutions are obtained by reversing the arc-length variable  $s \mapsto -s$ ). In this special reference frame, it is possible to represent the curve analytically using cylindrical coordinates  $\mathbf{x}(s) = (r \cos \varphi, r \sin \varphi, z)$ , where  $r(s)$ ,  $\varphi(s)$  and  $z(s)$  are functions of arc-length. Indeed, since  $\mathbf{x} = r\hat{r} + z\hat{z}$  and  $\mathbf{A} \times \mathbf{J} = 0$  in this special reference frame, the radial coordinate is immediately deduced from

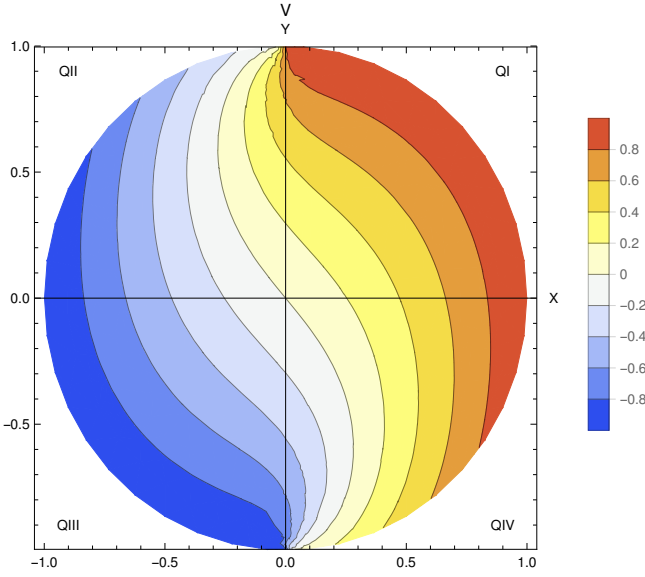


FIG. 2. Contours of constant  $V$  under the closure condition  $\Delta z = 0$ .

the square of the vector field  $\mathbf{I}$ ,

$$I^2 = \kappa^2 + \lambda_2^2 = J^2(r^2 + a^2) \iff r(s) = \sqrt{\frac{\kappa^2 + \lambda_2^2 - a^2 J^2}{J^2}}. \quad (35)$$

Somewhat counter-intuitively, the extrema of the curvature function and the major radius of the curve occur at the same points. We list:

$$r_{max}^2 = \frac{\kappa_0^2 p^2 + V^2}{J^2 w^2}, \quad r_{min}^2 = \frac{\kappa_0^2 V^2}{J^2 w^2}. \quad (36)$$

We note that when  $V = 0$ ,  $r_{min} = 0$ , and the curve self-intersects on the vertical  $z$ -axis.

Expressing the tangent vector as  $\mathbf{t}(s) = \mathbf{x}' = r' \partial_r \mathbf{x} + \varphi' \partial_\varphi \mathbf{x} + z' \partial_z \mathbf{x} = r' \hat{r} + r \varphi' \hat{\varphi} + z' \hat{z}$ , one obtains a differential equation for the vertical coordinate,

$$z' = \mathbf{t} \cdot \hat{z} = \mathbf{t} \cdot \frac{\mathbf{J}}{J} = \frac{\kappa^2 - 2\lambda_1}{2J}, \quad (37)$$

as well as for the toroidal angle,

$$\mathbf{I} \cdot \mathbf{t} = \lambda_2 = aJz' - Jr^2 \varphi', \quad (38)$$

which we express as

$$\frac{d\varphi}{dt} = \frac{awJ}{\kappa_0} \frac{\kappa^2 - 2\lambda_1 - 2\lambda_2/a}{\kappa^2 + \lambda_2^2 - a^2 J^2} = U + \frac{N}{1 - M \text{sn}^2(t, p)}, \quad (39)$$

where the following parameters are defined:

$$M = \frac{p^2}{p^2 + V^2}, \quad (40)$$

$$N = U \left( \frac{1 - R^2}{2(p^2 + V^2)} - 1 \right) - \frac{4w^2 \bar{J} X}{2(p^2 + V^2)}. \quad (41)$$

Analytic solutions of the differential equations (37) and (39) exist in terms of Jacobi theta functions [14].

The following useful identity can be proven (see appendix A):

$$N^2 = \frac{(1 - M)(M - p^2)}{M} = V^2(1 - p^2 - V^2), \quad (42)$$

indicating that  $p^2 \leq M \leq 1 \iff 0 \leq V^2 \leq 1 - p^2$ , as well as the fact that  $N = 0$  when  $V = 0$  and  $|V| = p'$  (independent of  $X$  and  $Y$ ).

By the property (20), the curvature vector is expressed in terms of the cylindrical coordinates as

$$\begin{aligned} \kappa \mathbf{n} &= \kappa \mathbf{b} \times \mathbf{t} = \mathbf{A} \times \mathbf{t} + (\mathbf{x} \times \mathbf{J}) \times \mathbf{t} \\ &= -rJ(a\varphi' + z')\hat{r} + r'J(a\hat{\varphi} + r\hat{z}). \end{aligned} \quad (43)$$

This vector is purely radial at extremal points where  $\kappa' = r' = 0$ . Evidently, the normal vector is always pointing radially inwards at the maximum radial position ( $t = 0$ ),

$$\mathbf{n} \cdot \hat{r}|_{r_{max}} = -1. \quad (44)$$

After some tedious and uninteresting algebra starting from (43), it is found that the direction of the normal vector at the minimal radial position depends only on the sign of  $Y$  and  $V$ ,

$$\mathbf{n} \cdot \hat{r}|_{r_{min}} = \text{sgn}(V)\text{sgn}(Y), \quad (45)$$

where  $\text{sgn}(Y) = Y/|Y|$ ,  $\text{sgn}(V) = V/|V|$ .

## VI. CLOSURE CONDITIONS

### A. Periodicity of curvature

The curvature, the torsion and the radial coordinate of the solution curves are periodic functions in  $t$  by virtue of  $\text{sn}(t + 2K(p), p) = -\text{sn}(t, p)$ , where  $K(p)$  is the complete elliptic integral of first kind. Their period in the arc-length variable  $s$  defines the fundamental length  $l$ ,

$$\kappa_0 l = 4wK(p). \quad (46)$$

Periodicity of the curvature and torsion functions however does not guarantee that the curve is closed. The helix is an example of a non-closing curve where the constant curvature and torsion functions are trivially periodic. As it will be seen in the following, there are in fact no non-planar closed solution curves with the same periodicity as the curvature function. Closed  $C^\infty$ -curves may however occur when one lets the parameter  $s \in [0, nl]$  extend over an integer multiple  $n \in \mathbb{N}^*$  of the fundamental length, thereby stringing together identical segments of length  $l$ , and requiring that i) the vertical displacement vanishes and ii) the toroidal angle returns to the same value modulo  $2\pi$ . The total length of the curve is then  $L = nl$  (and the integer  $n$  can be treated as a dependent variable of  $X$ ,  $Y$  and  $p^2$ ).

### B. Vertical displacement

By requiring that the net vertical displacement vanishes,  $\int_0^L z' ds = z(L) - z(0) = \Delta z = 0$ , the first closure condition is obtained as

$$\langle \kappa^2 \rangle = 2\lambda_1, \quad (47)$$

where

$$\langle \kappa^2 \rangle = \frac{1}{L} \int_0^L \kappa^2 ds = \frac{\kappa_0^2}{w^2} \left( w^2 + \frac{E(p)}{K(p)} - 1 \right). \quad (48)$$

This closure condition does not depend on the size of the curve (adimensional) and determines the value of  $p^2$  as a function of  $X$  and  $Y$  through

$$X^2 + Y^2 = U^2 + V^2 = R^2 = A(p) \quad (49)$$

where

$$A(p) = 2 \frac{E(p)}{K(p)} - 1. \quad (50)$$

The function  $A(p)$  monotonically decreases from  $A(0) = 1$  to  $A(1) = -1$ , passing through zero at  $p_{max}^2 = 0.8261 \dots$ . The  $(X, Y)$  parameters defining curves whose end-points are at the same height are thus conveniently limited to the unit disk. Although more stringent bounds exist, it is useful to note that  $A < 1 - p^2 = p'^2$ ,  $\forall p > 0$ .

The closure condition implies that  $z' = (\kappa^2 - \langle \kappa^2 \rangle)/2J$  has a purely oscillatory behaviour, zero mean and the same periodicity as the curvature function, i.e.  $z(s)$  crosses zero twice per segment where  $r(s)$  is extremal. The vertical coordinate has thus one maximum and one minimum per segment, alternating between the extrema of the radial coordinate. The projection on the  $(r, z)$  plane is therefore isotopic to a circle; the solution curves are embedded on tori of revolution under the first closure condition. Closed curves on this torus represent a set of measure zero in the parameter space  $(X, Y)$ .

The edge of the unit disk corresponds to  $p \rightarrow 0$ ,  $K \rightarrow \pi/2$ ,  $w \rightarrow |Y|$ ,  $X^2 \rightarrow 1 - Y^2$ ,  $M \rightarrow 0$  and features curves with constant curvature  $\kappa \rightarrow \kappa_0 = 2\pi n|Y|/L$  and constant toroidal variation  $d\varphi/dt \rightarrow U + N$ . The torsion function is therefore also constant and equal to

$$\tau \xrightarrow{p \rightarrow 0} \frac{2\pi n}{L} |X| \frac{\text{sgn}(X) + \text{sgn}(Y)}{2} \quad (51)$$

where  $\text{sgn}(X) = X/|X|$ .

At the edge of the unit disk in the first and third quadrants (QI and QIII), the torsion function  $\tau \rightarrow \kappa_0|X|/|Y|$  is non-zero, yielding helices. The radial excursion of the curves  $r_{max} - r_{min} \rightarrow 0$  however shrinks to zero at the same time as  $\bar{J} \rightarrow 0 \Rightarrow r_{min}\kappa_0 \rightarrow \infty$ . To respect the finite length condition, the curvature and torsion function must therefore diverge  $\kappa_0, \tau \rightarrow \infty$  (at fixed ratio). It can be shown that  $|U| \rightarrow 0, |V| \rightarrow 1$  at the edge of QI

and QIII, such that  $|N| \rightarrow 0$  and the toroidal excursion vanishes,  $d\varphi/dt \rightarrow 0$ . Consequently, the number of segments needs to diverge  $n \rightarrow \infty$  in order to form closed curves. The limiting solution curves in QI and QIII are somewhat pathological and uninteresting for the design of stellarators.

At the edge of the unit disk in the second and fourth quadrants (QII and QIV), the torsion function vanishes, yielding planar circular curves. One can show that  $U \rightarrow Y, V \rightarrow X$  and  $N \rightarrow Y$ , yielding a finite toroidal displacement per segment of  $\Delta\varphi/2\pi n \rightarrow Y$ . The solution curves at the edge of QII and QIV thus trivially close, provided that  $Y$  is a rational number.

### C. Toroidal displacement

The second closure condition requires that the variation in the cylindrical angle at the end of one segment be a rational fraction  $m/n$  of  $2\pi$  so that, by combining  $n$  identical segments, the curve closes after  $m$  revolutions around the vertical axis. The condition  $\Delta\varphi/2\pi n = m/n$  leads to a countably infinite family of relations between  $X, Y$  and  $p^2$ , labelled by the integer pair  $\{(m, n) | |m| < |n|\}$ . For the design of the magnetic axis of stellarators, we are mostly interested in curves that close after only one revolution around the vertical axis, i.e.  $m = 1$ . Knotted configurations [18] would correspond to  $m > 1$ .

The toroidal displacement per segment can be expressed in terms of elliptic integrals of third kind  $\Pi(\alpha^2, p)$  (see appendix B). The expression is valid for any choice of parameters  $(X, Y, p^2)$  and reduces thanks to identity (42) to

$$\begin{aligned} \frac{\Delta\varphi}{2\pi n} &= \frac{1}{2\pi} \int_0^{2K} \frac{d\varphi}{dt} dt = \frac{1}{2} \left[ \frac{UK}{\pi/2} + \frac{N}{\pi/2} \Pi(M, p) \right] \\ &= \frac{1}{2} \left\{ \frac{UK}{\pi/2} + \frac{\text{sgn}(N)}{\pi/2} [KE(\xi, p') - (K - E)F(\xi, p')] \right\}, \end{aligned} \quad (52)$$

where  $\text{sgn}(N) = N/|N|$ ,  $F(\xi, p)$  is the incomplete elliptic integral of first kind,  $K = K(p) = F(\pi/2, p)$ ,  $E(\xi, p)$  is the incomplete elliptic integral of second kind,  $E = E(p) = E(\pi/2, p)$  and the  $\xi$  angle satisfies

$$\cos \xi = \sqrt{\frac{p^2(1 - M)}{p^2 M}} = \sqrt{\frac{V^2}{1 - p^2}}. \quad (53)$$

This closure condition again does not depend on the size of the curve.

The toroidal displacement per segment  $\Delta\varphi/2\pi n$  is a continuous function away from  $N = 0$ , where either  $V$  crosses zero,  $|V| \rightarrow 0$ , or  $V$  reaches its limiting amplitude,  $|V| \rightarrow p'$ . There is no problem in the latter case since  $\xi \rightarrow 0$  and  $\Delta\varphi \rightarrow 2nUK$  (under the first closure condition, this uninterestingly happens only on the edge of the unit disk in QI and QIII where  $|V| \rightarrow 1$  and  $|U| \rightarrow 0$ ). In the

former however,  $\xi \rightarrow \pi/2$ , and the Legendre relation,

$$K(p)E(p') + E(p)K(p') - K(p)K(p') = \pi/2, \quad (54)$$

implies that the toroidal displacement per segment tends to

$$\frac{\Delta\varphi}{2\pi n} \xrightarrow{|V| \rightarrow 0} \frac{1}{2} \left[ \frac{UK}{\pi/2} + \text{sgn}(N) \right]. \quad (55)$$

The toroidal displacement per segment is thus discontinuous crossing through the  $V = 0$  line, where the curves self-intersect at  $r = 0$ . The jump is exactly 1.

Assuming that the first closure condition  $\Delta z = 0$  is in place, it turns out that  $\text{sgn}(N) = -\text{sgn}(V)$ . Figure 3 displays the contours of  $\Delta\varphi/2\pi n$  at the values  $\pm 1/2, \pm 1/3, \pm 1/4, \pm 1/5, \pm 1/6$  and at the complimentary values  $\pm 2/3, \pm 3/4, \pm 4/5, \pm 5/6$ . It is observed that one can deform a closed  $(-m, n)$ -curve starting at  $Y = -m/n$  in QIV into a  $(n-m, n)$ -curve arriving at  $Y = 1-m/n$  in QII by following a rational contour of  $\Delta\varphi/2\pi n$ . In particular, starting from a once-covered circle on the edge of the unit disk in the fourth quadrant at  $(X, Y) = (\sqrt{n^2 - 1}/n, -1/n)$ , the curve can be deformed into an elastic rod where the contour-line intersect the  $X$ -axis ( $Y = 0$ ), followed by an elastica where the contour-line intersects the  $Y$ -axis ( $X = 0$ ), then into a self-intersecting curve with  $n$  lobes where the contour-line crosses the  $V = 0$  line, then a  $(n-1, n)$  torus knot in the second quadrant where  $V < 0$  line, and finally into an  $(n-1)$ -covered circle (knotted) at the boundary of the second quadrant at  $(X, Y) = (\sqrt{2n-1}/n, 1-1/n)$ . The movies in the supplementary material show this sequence for the  $n = 3$  and  $n = 5$  family of closed elastic curves.

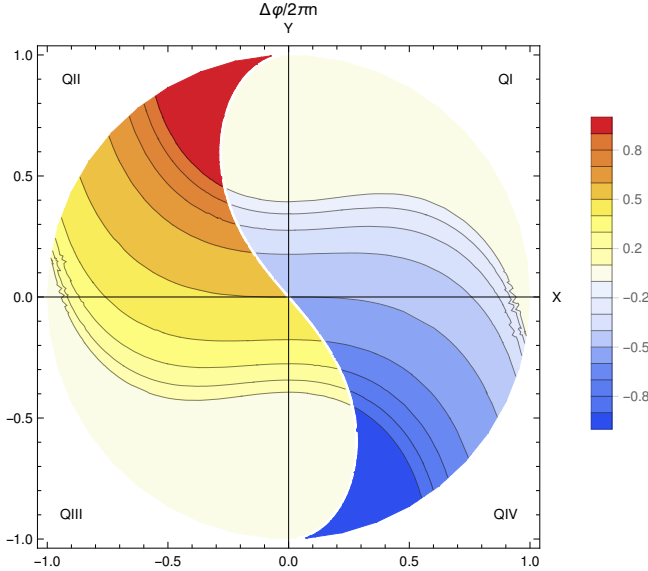


FIG. 3. Level curves of the toroidal displacement  $\Delta\varphi/2\pi n$  under the closure condition  $\Delta z = 0$  at the values  $\pm 1/2, \pm 1/3, \pm 1/4, \pm 1/5, \pm 1/6$  and at the complimentary values  $\pm 2/3, \pm 3/4, \pm 4/5, \pm 5/6$ .

## VII. LINKING, TWISTING AND WRITHING OF CURVES AND MAGNETIC FIELDS

The average torsion over multiples of the fundamental length can be expressed in terms of elliptic integrals of third kind. The result holds for both open and closed solution curves of the Euler-Lagrange equations and arbitrary parameters  $(X, Y, p^2)$ .

In the case where  $p^2 < w^2$ , i.e.  $|Y| > 0$ ,

$$\langle \tau \rangle = \frac{1}{L} \int_0^L \tau ds = \frac{1}{K} \int_0^K \tau dt = \frac{\kappa_0}{2} \left[ \bar{\lambda}_2 + \bar{c} \frac{\Pi\left(\frac{p^2}{w^2}, p\right)}{K} \right], \quad (56)$$

and hence the integrated torsion is

$$\mathcal{T}_{w, \text{Frenet}} = \frac{n}{2} \left\{ \frac{XK}{\pi/2} + \frac{\text{sgn}(Y)}{\pi/2} [KE(\chi, p') - (K - E)F(\chi, p')] \right\}, \quad (57)$$

where the  $\chi$  angle satisfies

$$\sin \chi = \frac{w'}{p'} = \sqrt{\frac{1-w^2}{1-p^2}} = \sqrt{1 - \frac{Y^2}{1-p^2}}. \quad (58)$$

Figure 4 shows a contour plot of the integrated torsion per segment  $\mathcal{T}_{w, \text{Frenet}}/n$  on the  $(X, Y)$  unit disk where the closure condition  $\Delta z = 0$  is imposed to define the value of  $p^2$  (see section VIB).

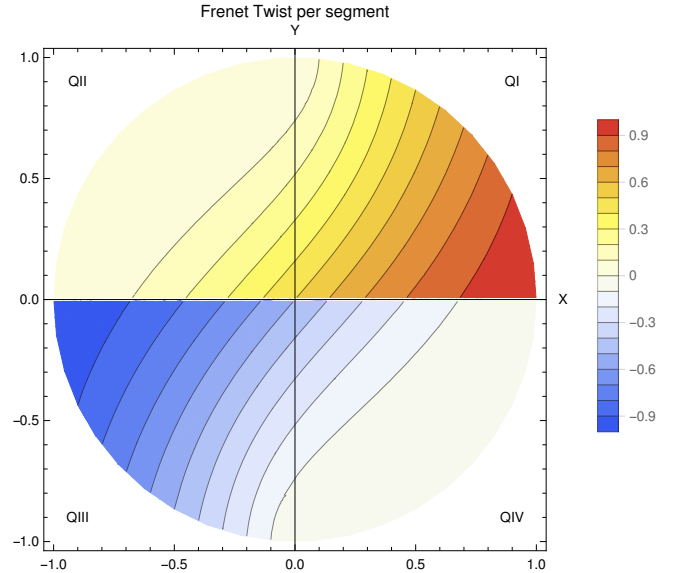


FIG. 4. Integrated torsion per segment  $\mathcal{T}_{w, \text{Frenet}}/n$  of a solution curve under the closure condition  $\Delta z = 0$ .

As  $|Y| \rightarrow 0$ ,  $p^2 \rightarrow w^2$  and  $\chi \rightarrow \pi/2$ , the Legendre relation implies that the integrated torsion tends to

$$\mathcal{T}_{w, \text{Frenet}} \xrightarrow{|Y| \rightarrow 0} \frac{n}{2} \left[ \frac{XK}{\pi/2} + \text{sgn}(Y) \right]. \quad (59)$$

and is discontinuous as  $Y$  changes sign. The jump is exactly  $n$ . For the special case of elastic rods,  $p^2 = w^2 \iff c = Y = 0$ , the constant torsion function is held at the intermediate value

$$\tau|_{Y=0} = \frac{\lambda_2}{2} = \frac{n}{2} \frac{XK}{\pi/2} \frac{2\pi}{L}. \quad (60)$$

In this case, the curvature function touches zero (and its derivative is discontinuous) at exactly  $n$  inflexion points along the curve. Although the curve itself is smooth and well-defined, its representation via the Frenet frame breaks down. It is tempting to believe, in light of Mercier's formula [6], that the discontinuity of the integrated torsion in equation (59) has a physical impact on the on-axis rotational transform of a magnetic field, but this would be ignoring the role of the *integer of topological origin* [7]. This number actually corresponds to the linking of the Frenet frame,  $\mathcal{L}_{k,\text{Frenet}}$ , i.e. how many times the normal vector wraps around the curve. It is an integer  $\mathcal{L}_{k,\text{Frenet}} = Z \in \mathbb{Z}$  for closed periodic curves and a topological invariant of the Frenet framing.

In [19, 20], it is demonstrated by continuously deforming a generic curve through states of inflexion that both the integrated torsion  $\mathcal{T}_{w,\text{Frenet}}$  and the linking of the Frenet frame  $\mathcal{L}_{k,\text{Frenet}}$  are discontinuous functions. Fortunately however, the jump has to be exactly the same for both functions such that their difference, the so-called Writhe,

$$\mathcal{L}_{k,\text{Frenet}} - \mathcal{T}_{w,\text{Frenet}} = Z - \frac{L}{2\pi} < \tau > = \mathcal{W}_{r,\text{Frenet}}, \quad (61)$$

is a smoothly varying function across a state of inflexion. This is a corollary of the well-celebrated Călugăreanu theorem [21] applied to the Frenet frame. The Writhe is a geometric property of the curve, which is well-defined in the presence of inflexion points or straight segments. It represents the average crossing number over all projections and can be evaluated via a double Gauss integral [22]. Most importantly, the Writhe is independent of the framing of the curve, i.e.  $\mathcal{W}_{r,\text{Frenet}} = \mathcal{W}_r$ .

The Călugăreanu theorem acquires a special interpretation when used to quantify how many times a neighbouring field-line links to the magnetic axis,

$$\mathcal{L}_k = \mathcal{W}_r + \mathcal{T}_w = \mathcal{L}_{k,\text{Frenet}} - \mathcal{T}_{w,\text{Frenet}} + \mathcal{T}_w, \quad (62)$$

i.e. the field-line linking (not necessarily integer) is equal to the linking of the Frenet frame **minus** the integrated torsion of the axis, plus the Twist  $\mathcal{T}_w$  of the magnetic field. The Twist of the magnetic field can be shown to originate independently and almost exclusively from parallel current (curl) and the rotation of the elliptical boundary. This statement will be further detailed in a future publication. The important message is that the physically relevant quantity for the on-axis rotational transform in relation to non-planar geometry is the **Writhe** of the magnetic axis.

A standard definition of the rotational transform is the average linking of neighbouring field-lines per toroidal

revolution, i.e.  $\mathcal{L}_k$  divided by the total toroidal displacement of the curve,

$$\frac{\iota}{2\pi} := \frac{\mathcal{L}_k}{\Delta\varphi} \sim \frac{\mathcal{W}_r}{\Delta\varphi}. \quad (63)$$

The presence of the integrated torsion in Mercier's formula appears to be, in light of equation (62), an artefact of the Frenet frame. Expression (63) is noted to be suitable for vacuum fields (no parallel currents) surrounded by a circular boundary where the Twist of the magnetic field can be neglected.

To work out the Writhe of the unknotted closed solution curves along the level contour  $\Delta\varphi/2\pi n = -1/n$ , we start at the edge of QIV at  $(X, Y) = (\sqrt{n^2 - 1}/n, -1/n)$  where the curve is composed of  $n$  planar arc-lengths forming a (once-covered) circle. Since  $Y < 0$  and  $V > 0$  along  $\Delta\varphi/2\pi n = -1/n$ , the normal vector never points outwards (see equation 44 and 45) such that the neighbouring curve  $\mathbf{x}(s) + \epsilon \mathbf{n}(s)$  easily detaches from  $\mathbf{x}(s)$ ,  $\forall \epsilon$ . This implies that the Frenet frame is not linking, and the integer  $Z = 0$ . The Writhe  $\mathcal{W}_r = -\mathcal{T}_{w,\text{Frenet}}$  is simply minus the integrated torsion along the level contour  $\Delta\varphi/2\pi n = -1/n$  where  $Y < 0$ , and for these solution curves, the rotational transform matches the integrated torsion identically,

$$\iota^0 = \mathcal{T}_{w,\text{Frenet}}. \quad (64)$$

The integrated torsion is negative in QIV, vanishing at the edge of the unit disk. The subsequent vanishing of the Writhe is consistent with the fact that, for planar curves, the Writhe is equal to the number of crossings, and the once-covered circle is devoid of them.

Passing through the  $Y = 0$  line into QI, the solution curves experiences  $n$  inflexion points where the curvature vector vanishes. Because the integrated torsion jumps by  $+n$  but the Writhe must remain continuous, we deduce that the Frenet frame must link by the same amount, i.e.  $Z = n$ . Indeed, when  $Y > 0$  along  $\Delta\varphi/2\pi n = -1/n$ , the normal vector points radially inwards at  $r_{\max}$  but outwards at  $r_{\min}$ . Knowing that the solution curve lies on a torus of revolution, the neighbouring curve  $\mathbf{x}(s) + \epsilon \mathbf{n}(s)$  behaves as the torus' centre line, and is being linked once per periodicity by  $\mathbf{x}(s)$ . The Writhe of closed solution curves is thus  $\mathcal{W}_r = n - \mathcal{T}_{w,\text{Frenet}}$  along  $\Delta\varphi/2\pi n = -1/n$  where  $Y > 0$ . The rotational transform is then given by

$$\iota^+ = -n \left( 1 - \frac{\mathcal{T}_{w,\text{Frenet}}}{n} \right). \quad (65)$$

The level contour  $\Delta\varphi/2\pi n = -1/n$  ends in QII on the  $V = 0$  line, where closed solution curves self-intersect at the origin of the cylindrical axis. The level contour however connects with that of  $\Delta\varphi/2\pi n = (n-1)/n$  in the region where  $V < 0$ , yielding a continuous deformation (homotopy) from unknotted solutions to  $(n-1, n)$ -torus knots in QII. As a particular case of the general formula  $C = \min[(p-1)q, (q-1)p]$  for the number of crossings of



$(p, q)$ -torus knots, the conjugate solution curves feature  $C = (n - 2)n$  crossings (all negative). They tend to  $(n - 1)$ -covered flat circles at the edge of the unit disk in QII, where the torsion vanishes. Consequently, the value of the Writhe approaches  $-C$  and we deduce that the Frenet linking is  $Z = -C = n(2 - n)$  along the entire level contour  $\Delta\varphi/2\pi n = (n - 1)/n$ . In QII where  $V < 0$ , the Writhe is thus  $\mathcal{W}_r = n(2 - n) - \mathcal{T}_{w, \text{Frenet}}$  and the rotational transform (63) reads

$$\iota^- = -n \left( \frac{n-2}{n-1} + \frac{\mathcal{T}_{w, \text{Frenet}}}{n(n-1)} \right). \quad (66)$$

Expression (66) has the disadvantage that  $\iota^-$  tends to the finite value  $n(n - 2)/(n - 1)$  at the edge of QII, where the knot becomes a  $(n - 1)$ -covered circle. This conflicts with the idea that rotational transform measures on a Poincaré plot the poloidal increment  $\Delta\theta$  of neighbouring field-lines around the magnetic axis,  $\iota/2\pi = \Delta\theta/\Delta\varphi$ ; field-lines that follow the Frenet frame are fixed points on a Poincaré plot and do not progress poloidally, i.e.  $\Delta\theta \propto \iota \rightarrow 0$  is expected to vanish at the edge of QII. For knotted configurations, it thus seems logical to offset the definition of rotational transform by the linking of the curve with respect to a fixed axis, e.g. the vertical axis. The latter choice is known as the *blackboard framing* and yields the so-called *Kaufmann self-linking number*  $\mathcal{L}_S$  [23]. The effective rotational transform per curve periodicity is now defined as

$$\iota_{\text{eff}} := \mathcal{L}_k - \mathcal{L}_S \sim \mathcal{W}_r - \mathcal{L}_S \quad (67)$$

The prescription (67) suits unknotted configurations, where  $\mathcal{L}_S = 0$ , so that results (64) and (65) remain unchanged. The Frenet and blackboard framings coincide at the edge of the unit disk, so that for knotted solution curves  $\mathcal{L}_S = \mathcal{L}_{k, \text{Frenet}} = \mp C$  and we obtain

$$\iota_{\text{eff}}^- = -\mathcal{T}_{w, \text{Frenet}}. \quad (68)$$

The integrated torsion  $\mathcal{T}_{w, \text{Frenet}}$  is continuous across the  $V = 0$  line, as seen on figure 4, so the jump  $n(n - 1)$  in the Frenet linking must therefore compensate the jump in the Writhe, again by the Călugăreanu theorem. Figure 5 summarises the behaviour of the integrated torsion per segment  $\mathcal{T}_{w, \text{Frenet}}/n$ , the Frenet linking per segment  $\mathcal{L}_{k, \text{Frenet}}/n$ , the Writhe per segment  $\mathcal{W}_r/n$ , the toroidal displacement per segment  $\Delta\varphi/2\pi n$  and the on-axis rotational transform per segment  $\iota/n$  and  $\iota_{\text{eff}}/n$  as a function of the parameter  $X$  while deforming the  $n = 3$  family of solution curves along level contours  $\Delta\varphi/2\pi n = -1/3$  and  $\Delta\varphi/2\pi n = 2/3$ . The evolution is also illustrated in the supplementary material.

According to formulae (64-67), the rotational transform (purple curve on figure 5) reaches its extreme value at the  $V = 0$  line for any value of  $n$ . As shown on figure 6, the integrated torsion  $\mathcal{T}_{w, \text{Frenet}}|_{V=0} < 1$  is always smaller than unity on the  $V = 0$  line and decreases with the number of segments. Consequently, the on-axis rotational transform  $|\iota^+|_{\text{max}} > |\iota^-|_{\text{max}} > |\iota_{\text{eff}}^-|_{\text{max}}$  is greater

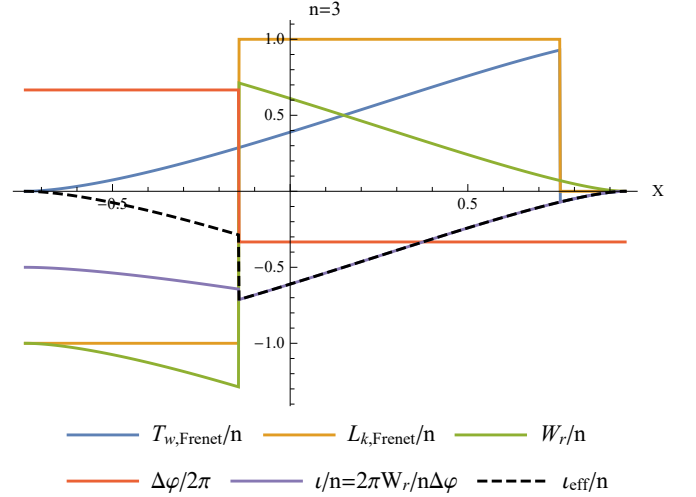


FIG. 5. Behaviour of the integrated torsion (blue), Frenet linking (orange), Writhe (green), toroidal displacement (red), on-axis rotational transform (purple) and effective rotational transform (dashed black) per segment for the  $n = 3$  family of closed solution curves as a function of the parameter  $X$ . The two discontinuities correspond to the crossing of the  $Y = 0$  line (on the right) and the  $V = 0$  line (on the left).

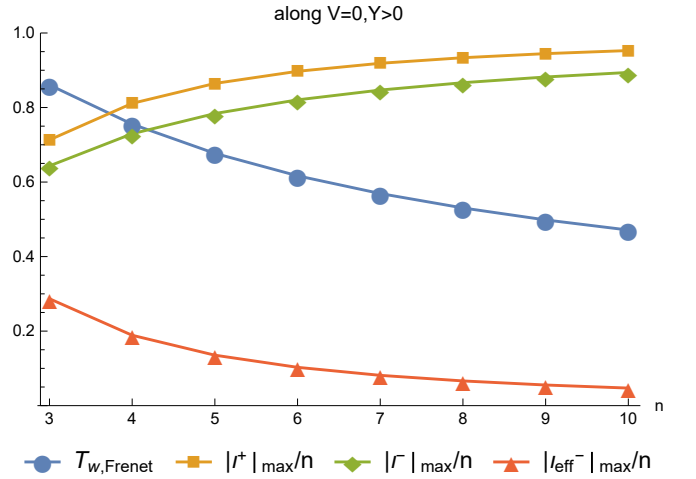


FIG. 6. (blue) Integrated torsion  $\mathcal{T}_{w, \text{Frenet}}$  along the  $V = 0$  as a function of the number of segments  $n$ . (orange) maximum achievable on-axis rotational transform per segment of unknotted configurations, (green) of the conjugate  $(n - 1, n)$ -torus knots, (red) maximum effective rotational transform of  $(n - 1, n)$ -torus knots per segment.

in absolute value for unknotted configurations than for knotted ones, as highlighted by the orange, green and red markers on figure 6.

## VIII. CONCLUSION

The benign question of finding closed curves with minimal bending energy but fixed integrated torsion led to the study of a rich class of elasticae. Several interesting discontinuities appear explicitly in the analytic solutions, which were given in terms of elliptic integral of third kind. The discontinuity of the integrated torsion, where the solution curves pass through a state of inflexion, is understood as an artefact of the Frenet frame. The discontinuity of the toroidal displacement per segment, where the solution curves self-intersect through the origin, is understood as an artefact of the cylindrical coordinate system. Thanks to the Călugăreanu theorem, one of the three relevant quantities, namely Writhe when crossing the  $Y = 0$  and Twist when crossing the  $V = 0$  line, remained continuous, thereby imposing the jumps in the other two to mutually cancel. Although everything could have been calculated explicitly, the strong constraint that is the Călugăreanu theorem helped deduce the Linking of the Frenet frame for all closed solution curves as well as quantify the rotational transform purely arising from the non-planar geometry of the magnetic axis.

Despite the obvious scaling of the on-axis rotational transform with the number of repeated segments  $n$ , it is found that the extremum of  $\iota/n$  is achieved by unknotted magnetic axes that are about to self-intersect. Whether these solutions can be realised by the vacuum fields of a coil design remains to be addressed. The detailed study of these optimal curves nevertheless highlights the leading role of the *Writhe* component. This fact is not ap-

parent from Mercier's formula but important to interpret figure 4, which deceptively shows that the maximum integrated torsion is achieved by a magnetic axis with constant torsion. The beneficial effect of Writhe suggests the possibility of designing plasmas with 5-10 times the on-axis rotational transform of current stellarators. The usual Fourier representation is unsuited to access such configurations through numerical optimisation since the toroidal angle will generally be a non-monotonic function of the axis' arc-length.

We conclude by noting that such optimal curves seem to occur in other natural phenomena such as the super-coiling of DNA [24], the vortices of under-water air bubbles [25], flux-tubes in the solar corona [26], etc... Results herein may be directly applicable to the interplay between Twist, Writhe and Linking in those systems.

## SUPPLEMENTARY MATERIAL

The supplementary material contains two movies illustrating the continuous deformation discussed in VIC of the  $n = 3$  and  $n = 5$  family of closed elasticae (in black) and the linking of the Frenet frame in the form of a curve (in red) displaced in normal direction.

## ACKNOWLEDGMENT

The authors would like to thank stimulating discussions related to this work with E.Hirvijoki, D.E.Ruiz, A.Brizard, N.Fowkes and S.I.Abarzhi.

- 
- [1] L. Spitzer, *The Physics of Fluids* **1**, 253 (1958).
  - [2] O. Sauter, M. A. Henderson, F. Hofmann, T. Goodman, S. Alberti, C. Angioni, K. Appert, R. Behn, P. Blanchard, P. Bosshard, R. Chavan, S. Coda, B. P. Duval, D. Fasel, A. Favre, I. Furno, P. Gorgerat, J.-P. Hogge, P.-F. Isoz, B. Joye, P. Lavanchy, J. B. Lister, X. Llobet, J.-C. Magnin, P. Mandrin, A. Manini, B. Marlétaz, P. Marmillod, Y. Martin, J.-M. Mayor, A. A. Martynov, J. Mlynar, J.-M. Moret, C. Nieswand, P. Nikkola, P. Paris, A. Perez, Z. A. Pietrzyk, R. A. Pitts, A. Pochelon, G. Pochon, A. Refke, H. Reimerdes, J. Rommers, E. Scavino, G. Tonetti, M. Q. Tran, F. Troyon, and H. Weisen, *Phys. Rev. Lett.* **84**, 3322 (2000).
  - [3] M. Kikuchi and M. Azumi, *Plasma Physics and Controlled Fusion* **37**, 1215 (1995).
  - [4] M. Landreman, *Nuclear Fusion* **57**, 046003 (2017).
  - [5] D. Gates, A. Boozer, T. Brown, J. Breslau, D. Curreli, M. Landreman, S. Lazerson, J. Lore, H. Mynick, G. Neilson, N. Pomphrey, P. Xanthopoulos, and A. Zolfaghari, *Nuclear Fusion* **57**, 126064 (2017).
  - [6] C. Mercier, *Nuclear Fusion* **4**, 213 (1964).
  - [7] P. Helander, C. D. Beidler, T. M. Bird, M. Drevlak, Y. Feng, R. Hatzky, F. Jenko, R. Kleiber, J. H. E. Proll, Y. Turkin, and P. Xanthopoulos, *Plasma Physics and Controlled Fusion* **54**, 124009 (2012).
  - [8] H. Yamada and al., *Nuclear Fusion* **51**, 094021 (2011).
  - [9] T. S. Pedersen, M. Otte, S. Lazerson, P. Helander, S. Bozhrenkov, C. Biedermann, T. Klinger, R. C. Wolf, H.-S. Bosch, and T. W. -X. Team, *Nature Communications* **7**, 13493 EP (2016).
  - [10] C. Zhu, S. R. Hudson, Y. Song, and Y. Wan, *Nuclear Fusion* **58**, 016008 (2018).
  - [11] S. Hudson, C. Zhu, D. Pfefferlé, and L. Gunderson, *Physics Letters A* **382**, 2732 (2018).
  - [12] J. Langer and D. A. Singer, *Journal of the London Mathematical Society* **s2-30**, 512 (1984).
  - [13] J. Langer and D. A. Singer, *SIAM Review* **38**, 605 (1996).
  - [14] T. A. Ivey and D. A. Singer, *Proceedings of the London Mathematical Society* **79**, 429 (1999).
  - [15] W. Fenchel, *Bull. Amer. Math. Soc.* **57**, 44 (1951).
  - [16] J. Langer and D. A. Singer, *Topology* **24**, 75 (1985).
  - [17] R. Dewar and S. Hudson, *Physica D: Nonlinear Phenomena* **112**, 275 (1998).
  - [18] S. R. Hudson, E. Startsev, and E. Feibush, *Physics of Plasmas* **21**, 010705 (2014).
  - [19] R. L. Ricca and H. K. Moffatt, "The helicity of a knotted vortex filament," in *Topological Aspects of the Dynamics of Fluids and Plasmas* (Springer Netherlands, Dordrecht, 1992) pp. 225–236.

- [20] H. K. Moffatt and R. L. Ricca, Proceedings of the Royal Society of London A: Mathematical, Physical and Engineering Sciences **439**, 411 (1992).
- [21] G. Călugăreanu, Rev. Math. Pures Appl. **4**, 5 (1959).
- [22] F. B. Fuller, Proceedings of the National Academy of Sciences **68**, 815 (1971).
- [23] W. F. Pohl, Journal of Mathematics and Mechanics **17**, 975 (1968).
- [24] K. Klenin and J. Langowski, Biopolymers **54**, 307.
- [25] D. Kleckner and W. T. M. Irvine, Nature Physics **9**, 253 EP (2013), article.
- [26] T. Török, B. Kliem, M. A. Berger, M. G. Linton, P. Démoulin, and L. van Driel-Gesztelyi, Plasma Physics and Controlled Fusion **56**, 064012 (2014).
- [27] P. Byrd and M. Friedman, *Handbook of elliptic integrals for engineers and scientists*, Grundlehren der mathematischen Wissenschaften (Springer-Verlag, 1971).

### Appendix A: Proof of identity (42)

Express  $\bar{J}$  as a function of  $\bar{\lambda}_1$ ,  $\bar{\lambda}_2$  and  $\bar{c}$  using equation (25)

$$\bar{J}^2 = \frac{1}{4}[(1 - 2\bar{\lambda}_1)^2 + (c - \bar{\lambda}_2)^2] \quad (\text{A1})$$

and  $\bar{a}$  from equation (21)

$$\bar{a} = \frac{2(c - 2\bar{\lambda}_1\bar{\lambda}_2)}{(1 - 2\bar{\lambda}_1)^2 + (c - \bar{\lambda}_2)^2} \quad (\text{A2})$$

From (23), express  $p^2$  as a function of  $\bar{\lambda}_1$ ,  $\bar{\lambda}_2$  and  $w^2$

$$p^2 = w^2[1 + \bar{\lambda}_2^2 + 2(1 - 2\bar{\lambda}_1)] - 1 \quad (\text{A3})$$

and then from (24)

$$w^4(c^2 + 4\bar{\lambda}_1 - \bar{\lambda}_2^2 - 2) - w^2(4\bar{\lambda}_1 - \bar{\lambda}_2^2 - 3) - 1 = 0 \quad (\text{A4})$$

Then

$$N^2 - \frac{(1 - M)(M - p^2)}{M} = \frac{4\bar{J}^2 \times \text{eq. (A4)}}{w^2(1 - 2\bar{\lambda}_1 - c\bar{\lambda}_2 + \bar{\lambda}_2^2)^2} \quad (\text{A5})$$

### Appendix B: Elliptic integral of third kind

According to [27, 413.01], the complete elliptic integrals of third kind can be expressed in terms of incomplete elliptic integral of first and second kind. For the case II (circular), i.e.  $p^2 < \alpha^2 < 1$ , one has

$$\Pi(\alpha^2, p) = \int_0^K \frac{dt}{1 - \alpha^2 \text{sn}^2(t, p)} \quad (\text{B1})$$

$$= \frac{\alpha[(E - K)F(\xi, p') + KE(\xi, p')]}{\sqrt{(\alpha^2 - p^2)(1 - \alpha^2)}} \quad (\text{B2})$$

where

$$\sin \xi = \sqrt{\frac{\alpha^2 - p^2}{\alpha^2 p'^2}} \quad p'^2 = 1 - p^2 \quad (\text{B3})$$

In particular,

$$\Pi(p^2, p) = \frac{E}{1 - p^2} \quad (\text{B4})$$

and

$$\Pi\left(\frac{p^2}{w^2}, p\right) = \frac{w[(E - K)F(\xi, p') + KE(\xi, p')]}{\sqrt{(1 - w^2)(w^2 - p^2)}} \quad (\text{B5})$$

for

$$\sin \xi = \sqrt{\frac{1 - w^2}{1 - p^2}} \quad (\text{B6})$$